Focal Mechanisms of the 2013 M_w 6.6 Lushan, China Earthquake and High-Resolution Aftershock Relocations

by Libo Han, Xiangfang Zeng, Changsheng Jiang, Sidao Ni, Haijiang Zhang, and Feng Long

Online Material: Tables of 1D velocity models and relocated events.

INTRODUCTION

The M_w 6.6 Lushan earthquake (hereafter referred to as the Lushan earthquake) occurred in the early morning on 20 April 2013 (Fig. 1). The earthquake caused more than 200 casualties, injured more than ten thousand people, and caused huge economic loss. This event was the most damaging earthquake in China since the 2008 **M** 8.0 Wenchuan earthquake and the 2010 **M** 7.1 Yushu earthquake.

The Lushan earthquake was widely felt as far as 500 km away, in an area of almost 1 million square kilometers. The area that suffered damage is also substantial (~20, 000 square kilometers). After five days of intensive field investigation, the intensity map was officially released based on the observed damage (http://www.cea.gov.cn/publish/dizhenj/464/478/20130425153642550719811/index.html, last accessed November 2013). The intensity map showed a northeast–southwest strike, and the maximum intensity was IX. The lengths of the long axis and short axis for the meizoseismal area are nearly 23 and 11 km, respectively, which agree well with rupture-process inversion results (Wang *et al.*, 2013).

The mainshock was well recorded by both local and global seismic networks, and the epicenter is located at latitude 30.3° N and longitude 103.0° E, which is about 80 km to the southwest of the epicenter of the 2008 Wenchuan earthquake. The shock occurred between the Pengguan fault (F3) and Dayi fault (F4) in the northeast-trending Longmenshan fault system (Fig. 1). The Longmenshan fault system lies along the eastern margin of the Tibetan plateau as a result of crustal extrusion against strong lithosphere of the Sichuan basin, which is part of the Yangtze block (Xu *et al.*, 2008). The Longmenshan fault system consists of four major faults from west to east, including the Wenchuan–Maowen fault, Beichuan fault, Pengguan fault, and Dayi fault (Densmore *et al.*, 2005). The unilateral rupture of the Wenchuan earthquake occurred along the Beichuan and Pengguan faults, and started at Yingxiu and propagated northeastward to Qingchuan (Zhang *et al.*, 2009). Although studies involving Coulomb Failure Stress suggest that earthquake hazard on the fault segments where the Lushan earthquake occurred should be enhanced after the Wenchuan earthquake (Parsons *et al.*, 2008), the community in the epicentral area was not well prepared for a big earthquake before the fifth anniversary of the Wenchuan earthquake.

Here, we report the preliminary results on the Lushan earthquake including relocation of aftershocks and source parameters of the mainshock and two large aftershocks. These results are helpful for understanding seismogenic and rupture processes of the earthquake.

SOURCE PARAMETERS OF THE MAINSHOCK

The double-couple solution of the mainshock was determined using the Cut-and-Paste algorithm (Zhao and Helmberger, 1994; Zhu and Helmberger, 1996). In the inversion, we used local seismograms from the China National Seismic Network (CNSN; Zheng *et al.*, 2010). Although nearly all the broadband stations within 250 km from the epicenter are clipped because of the large magnitude of the mainshock, *P* waves are still available for modeling at these distances. At larger distances, both *Pnl* and surface waves are well recorded (Fig. 2a).

The mainshock occurred near the boundary between the Eastern Tibet plateau and the Sichuan basin, across which substantial differences in crustal structure have been reported (Wang *et al.*, 2007; Li *et al.*, 2012; Zhang *et al.*, 2012). To account for lateral variation, we chose two 1D velocity models for computing Green's functions for paths in plateau and basin, respectively (Fig. 2b). The plateau model is taken from Zheng *et al.* (2009) and the basin model from Xie *et al.* (2012). Ⓔ Tables S1 and S2 (available as an electronic supplement to this paper) display the plateau and basin models, respectively. These velocity models are found to be effective in the focal mechanism inversions of the Wenchuan earthquake sequence and the 2010 Suining earthquake in Sichuan basin (Zheng *et al.*, 2009;

doi: 10.1785/0220130083

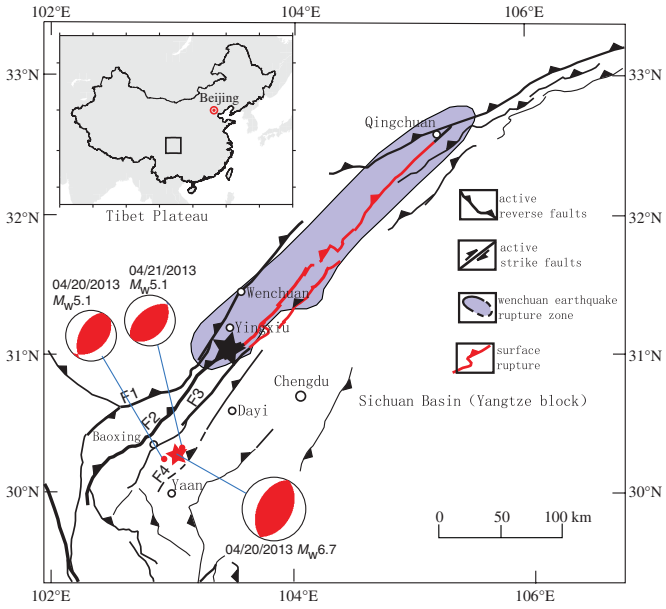

▲ **Figure 1.** Tectonic settings of Longmenshan fault system (after Zhang and Li, 2010; Liu *et al.*, 2013). Red star, Lushan earthquake epicenter; black star, Wenchuan earthquake epicenter. Lower hemisphere focal mechanisms of the mainshock and two **M**5+ aftershocks are also shown. The box on the inset marks the study region in mainland China. F1, Wenchuan–Maowen fault; F2, Beichuan fault; F3, Pengguan fault; F4, Dayi fault.

Luo *et al.*, 2011). The Green's functions were calculated with the frequency–wavenumber ($f-k$) technique (Zhu and Rivera, 2002) based on these two 1D models.

In the inversion, both the *Pnl* and surface-wave segments are bandpass filtered between 0.02 and 0.1 Hz. The 0.1 Hz frequency is probably low enough to account for the finite duration of the mainshock ($\sim M_w$ 6.6) according to scaling laws by Somerville *et al.* (1999). As displayed in Figure 2, the best waveform match is achieved at the depth of 12 km with the estimated magnitude M_w 6.7, which is consistent with NEIC and Global CMT results (M_w 6.6). The high cross-correlation coefficients (CCCs) between the synthetics and data suggest that the source parameters are well resolved. The strike, dip, and rake of the focal mechanism are 210°/47°/97°, respectively, and the auxiliary nodal plane solution is 20°/43°/83°. The focal mechanism indicates almost pure thrust rupture, consistent with the thrust nature of the Longmenshan fault system.

Teleseismic *P* waves provide even stronger constraints on the dip angle and depth of thrust events (Chen *et al.*, 2012). Here, we also invert source parameters of the mainshock using the teleseismic *P* waves (Fig. 3a). The focal mechanism obtained from teleseismic body-wave inversion was consistent with that from regional waveforms (Fig. 3b). Teleseismic inversion suggests a focal depth of 10 km, which is close to local waveform inversion.

The same approach was adopted to determine source parameters of strong aftershocks using local seismograms. Considering their moderate magnitudes in size, however, we use slight shorter period band-pass filters 0.02 ~ 0.15 Hz and 0.02 ~ 0.12 Hz for *Pnl* and surface-wave segments respectively. There are three **M**5+ aftershocks, but the first one occurred just five minutes after the mainshock. Therefore, it is difficult to obtain a reliable focal mechanism because of contamination from the coda of the mainshock. The focal mechanisms of the other two **M**5+ aftershocks are similar to the mainshock (Fig. 1), showing almost pure thrust. The detailed parameters of the mainshock and the two aftershocks including locations and focal mechanisms are listed in Table 1.

RELOCATIONS OF THE EARTHQUAKE AFTERSHOCK SEQUENCE

Usually, the aftershock distribution is capable of resolving the ambiguity between the rupture plane and auxiliary plane of point-source solutions. Event locations in the CNSN catalog were routinely determined from manual picks of *P*- and *S*-wave arrivals. Typical location error ranges from a few kilometers to dozens of kilometers, depending on the density of the seismic network. The catalog aftershock zone is about 30 km long and 15 km wide, thus it is necessary to relocate the sequence with higher location accuracy. Here we collected *P* and *S* arrival data of aftershocks (**M**2.5+) from the local seismic network in the first five days. In addition, portable stations were deployed after 22 April and their arrival data also were included for analysis.

The catalog locations are based on a 1D velocity model, which does not take into account the effect of substantial lateral velocity variation in our study region. To improve location accuracy, we first employed the hybrid velocity models (the two 1D models mentioned in the section on source inversion) and adopted Hypo2000 (Klein, 2002) to relocate the earthquake sequence. The relocated aftershocks show a more compact horizontal pattern than the catalog solution, and the sequence showed a nearly northeast strike of 30°, and alternatively a southwest strike of 210°. However, in the depth section, it is still difficult to tell whether the sequence dips to the west or east (Fig. 4a).

We further used the double-difference (DD) location method to better determine relative locations of the entire sequence (Waldhauser and Ellsworth, 2000). The method solves for event hypocenters and origin times using differential arrival time data from catalog phase picks and/or waveform cross correlations. An advantage of this method is that it is able to remove the common-path anomalies for each event pair observed at the same station. Considering the strong velocity heterogeneities in the study region, we adopted a modified version of the double-difference tomography code tomoDD, which calculates the travel times in a 3D velocity model using a spherical earth finite-difference travel time method (Zhang *et al.*, 2012). The 3D velocity model was developed with local *P* and *S* first arrival times in our study region and revealed strong lateral variations between tectonic units (Zhang *et al.*, 2012).

Previous studies have demonstrated advantages of DD relocation, for example, results from both synthetic- and real-data

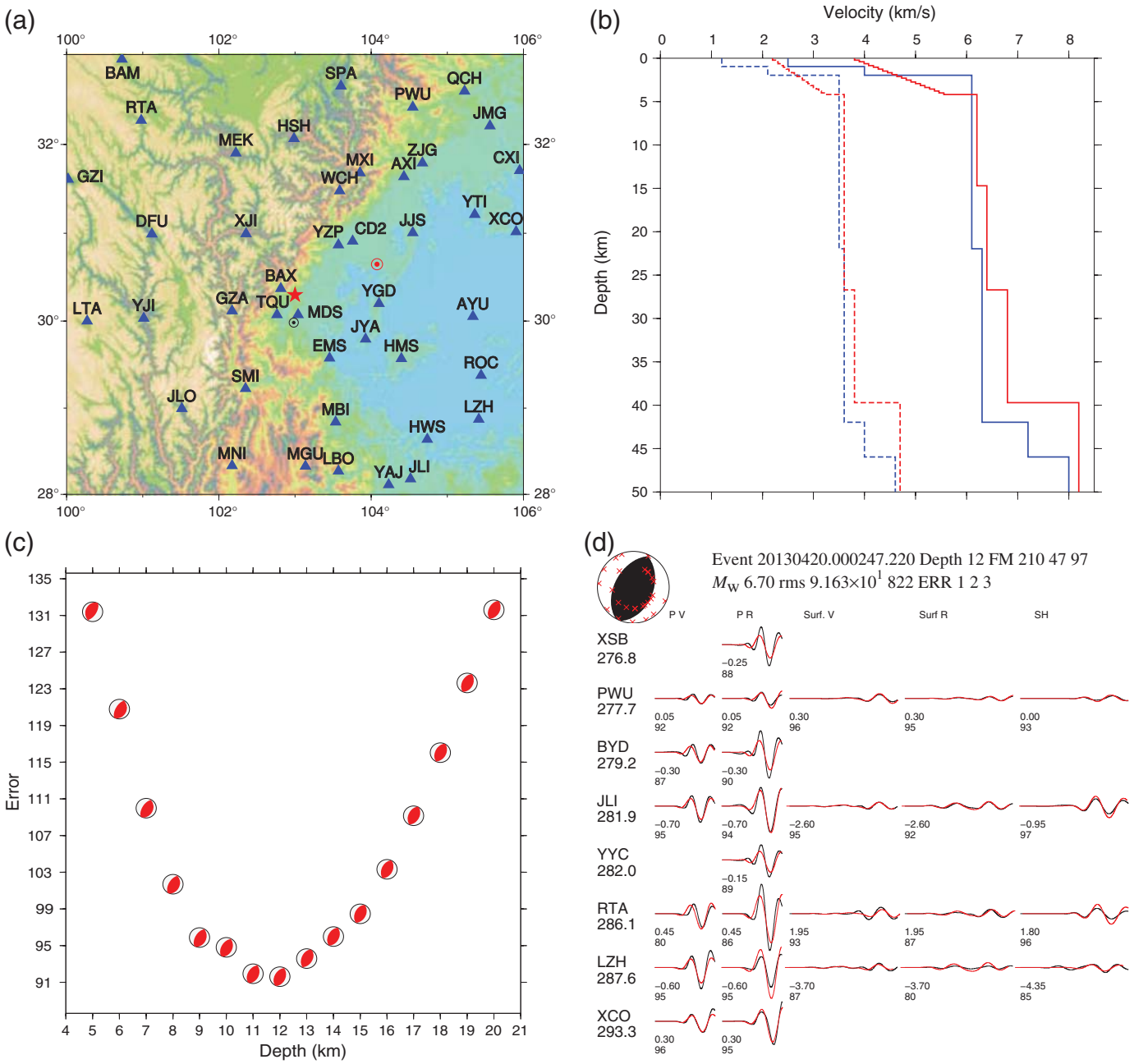

▲ **Figure 2.** (a) Local seismic stations used in waveform inversion. The red star, epicenter of the Lushan earthquake. (b) 1D Crustal velocity models used in the waveform inversion and relocation. The *S*- and *P*-wave velocities are shown as dashed lines and solid lines, respectively. Blue lines, plateau velocity model; red lines, basin model. (c) The misfit function versus focal depth. (d) Comparison between black, observed; and red, synthetic seismograms. The numbers below the station names are the epicentral distances in kilometers. The first number below each seismogram is the time shift between data and synthetics and the second number is the cross-correlation coefficient in percentage.

studies show that relative location errors are reduced by a factor of ~2 using catalog arrival times alone. Moreover, the errors can be further reduced by a factor of ~5–10 if differential times from cross correlations are used (Hauksson and Shearer, 2005). The CCC between all waveform pairs at the same station were then determined using a 2.5 s window beginning 0.5 s before the *P* arrival with a maximum time shift of 0.5 s. The time shift corresponding to the maximum CCC is treated as the differential arrival time between two events. Only event pairs with CCC greater than 0.70 were chosen for relocation. After the DD relocation, travel-time residuals for the catalog differential times and CCC times are ~40 and ~10 ms, respectively.

For each event pair, it requires at least eight links (or observations at the same station) during relocation. After

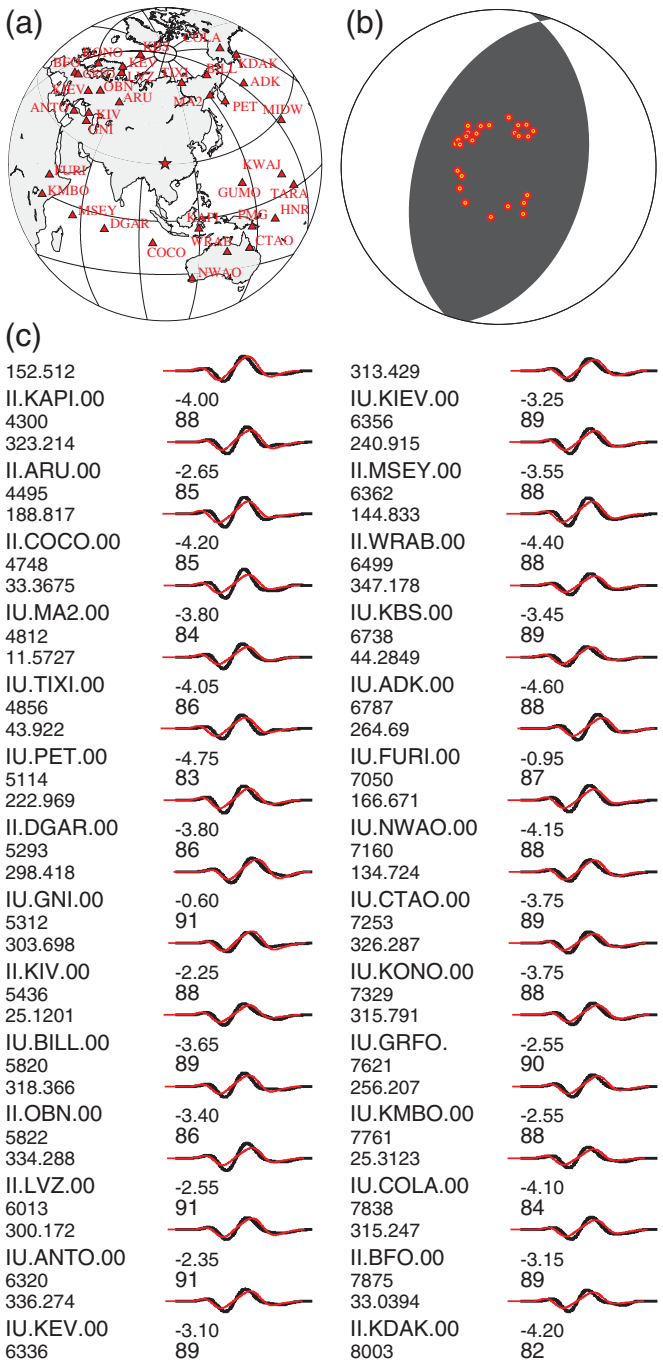

▲ **Figure 3.** (a) Teleseismic stations used in this study. Red star, epicenter of the Lushan earthquake. (b) Focal mechanism inverted from teleseismic *P*-wave data. (c) Comparison between black, observed and red, synthetic seismograms. The numbers below the station names are the epicentral distances in kilometers and the numbers above are the azimuths. See Figure 2 for more details.

relocation using tomoDD, in total 165 events were located and the rms travel-time residual for CCC times was reduced from 0.35 to about 0.01 s. The epicenter of the Lushan earthquake is found to be situated at 30.299° N, 102.964° E with hypocentral depth about 13 km (Fig. 4b). In order to analyze the depth pattern along the strike (30°) of the elongated aftershock zone, we project all the aftershocks along depth section AA′ (Fig. 5). Overall, the events located in the southern part were shallower than other parts, most of which are in the depth range of 8–12 km. In the central segment of AA′, the events are deeper than 10 and down to 20 km. In the northern segment, the depths of the events are more scattered than those in other segments.

For pure thrust events, the ruptured fault plane and auxiliary plane show the same strike. Therefore, it is necessary to resolve the ambiguity in depth section perpendicular to the strike (BB′, 120°). Obviously, the aftershocks as shown in box I delineate a fault dipping to the northwest and the dip angle of the fault plane is about 40°, which is close to that determined by waveform inversions using regional and teleseismic seismograms. Some aftershocks dipped southeast (box II, Fig. 5) may be related to a backthrust fault. In general, earthquakes with reverse faulting mechanism are followed by aftershocks on the hanging-wall block, rarely on the footwall block (Chang *et al.*, 2000; Huang *et al.*, 2008). Our relocation results confirmed this.

DISCUSSION AND CONCLUSION

We conducted waveform inversions using regional and teleseismic body-wave seismograms. A 12 km centroid depth of the mainshock was obtained using waveform inversion with regional seismograms, whereas the preferred centroid depth was 10 km when using only teleseismic body-wave records. Both results are close to the results of 12 km from joint inversion using regional and teleseismic waveform records (Zeng *et al.*, 2013) and 10 km from teleseismic body-wave inversions (Wang *et al.*, 2013).

The USGS body-wave moment tensor solution (http://earthquake.usgs.gov/earthquakes/eqarchives/fm/neic_b000gcdd_fmt.php, last accessed November 2013) for this event yields double-couple solution with the nodal planes angles (strike/dip/rake) 216°/47°/93° and 32°/43°/87°. Our focal mechanism results are consistent with the USGS solution. These solutions confirm that the Lushan earthquake is a thrust event. As compared to some continental thrust events such as the Wenchuan earthquake (33°) and the Northridge California earthquake (35°; Hauksson *et al.*, 1995), this earthquake occurred on a high dip-angle fault. But its dip angle is less than that of the 2003 San Simeon California earthquake (58°; Hardebeck *et al.*, 2004). Thus, it was difficult for the mainshock to rupture the surface. After relocation few aftershocks are found to occur above 8 km; this may imply that the fault rupture terminated at a depth of about 8 km. It is also suggested that a reverse fault with such a high dip angle would require high fluid pressure to accommodate slip failure (Sibson and Xie, 1998). The Lushan earthquake may be triggered by the buoyant migration of fluids similar to the case of the Wenchuan earthquake (Zhou and He, 2009).

The relocation results show that the mainshock and aftershocks predominantly occurred above 20 km in depth. In the epicentral area, the crustal thickness is about 46 km (Wang

Table 1
Locations and Focal Mechanisms of the Lushan Earthquake and its Two Largest Aftershocks

		Location from TomoDD			Magnitude		Focal Mechanisms			
Origin Date (yyyy/mm/dd)	Time UT (hh:mm:ss.ss)	Latitude (° N)	Longitude (° E)	Depth (km)	M_s	M_w	Strike (°)	Dip (°)	Rake (°)	Centroid Depth (km)
2013/04/20	00:02:47.22	30.299	102.964	13	7.0	6.7	210	47	97	12
2013/04/20	03:34:14.62	30.192	102.891	11	5.3	5.1	206	51	75	13
2013/04/21	09:05:22.76	30.331	103.006	13	5.4	5.1	232	52	99	12

et al., 2007). Thus, this sequence appears to have taken place in the upper crust. Usually, the seismicity is limited above the crustal brittle–ductile transition zone. In the Longmenshan fault zone, previous studies indicated that the brittle–ductile transition occurs at depths of 15 ~ 20 km (Zhou and He, 2009). Our relocation results are consistent with their studies. The relocated sequence suggests the ruptured fault dips to northwest. Combining this with the waveform inversion results, we propose that the nodal plane (strike 210°, dip 47°) is the ruptured fault plane.

The Lushan earthquake occurred in the southern part of the Longmenshan thrust belt. From west to east, there are four major faults: Gengda–Longdong (Wenchuan–Maowen), Yanjing–Wulong (Beichuan), Shuangshi–Dachuan (Pengguan), and Dayi faults. These faults extend to the northeast striking about 45° and dipping northwest with dip angles of 50°–70° at shallow depths (Yang *et al.*, 1999). There are also numerous folds that trend parallel to the main thrust faults near source regions (Jin *et al.*, 2010). Relocation results reveal that the sequence occurs between the Pengguan fault and the Dayi fault. Previous studies propose that Pengguan fault and Dayi fault are both active faults (Yang *et al.*, 1999; Densmore *et al.*, 2007). Although the surface projection of the dipping fault plane is close to the Dayi fault, there is a substantial gap of 5 km or so between them after taking the high dip angle of the faults into account. In addition, up to now no northeast–southwest-striking surface rupture has been reported. Therefore, the Lushan earthquake cannot be obviously associated with any identified surficial geological faults. It appears that the Lushan earthquake might have occurred on a blind thrust fault subparallel to the Dayi fault that is associated with the folds, similar to the 1994 M_w 6.7 Northridge, California, earthquake (Hauksson *et al.*, 1995). However, more studies including geodetic investigations are still needed to illuminate details of the rupture process and understand the seismogenic processes.

ACKNOWLEDGMENTS

Waveform data for this study were provided by the Data Management Center of China National Seismic Network at the

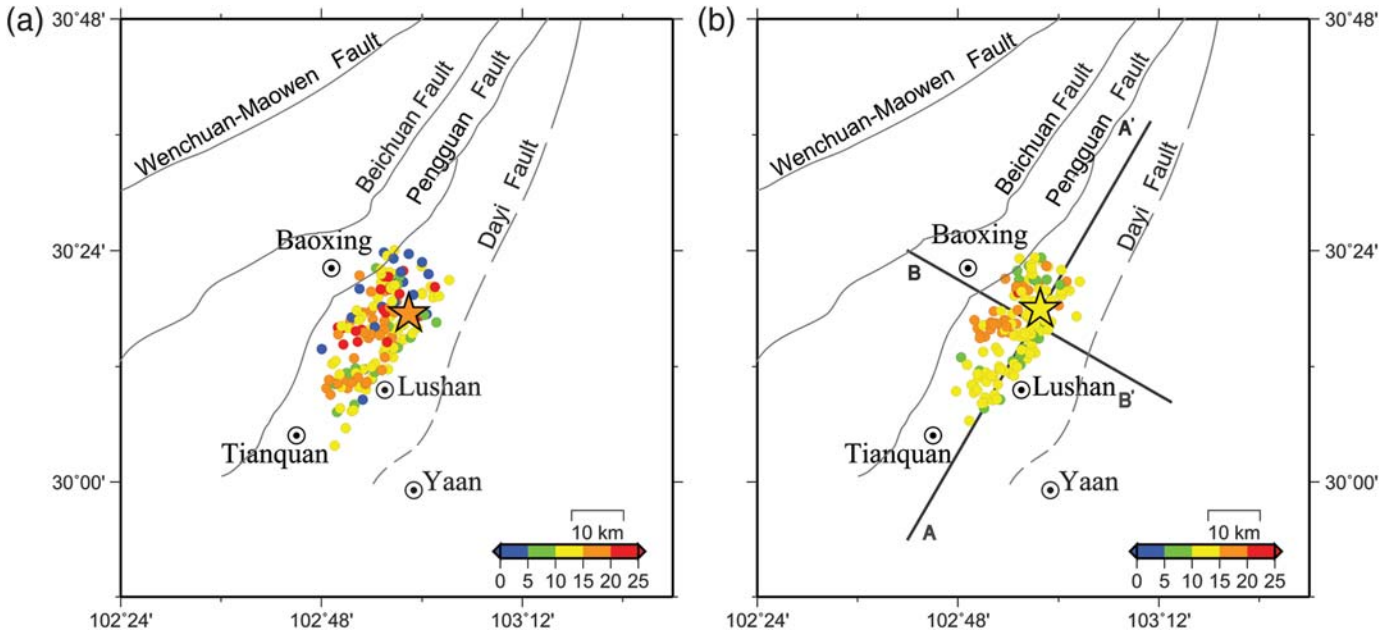

▲ **Figure 4.** (a) Map of relocated sequence (star, mainshock; circle, aftershock) with Hypo2000 method. Focal depth is indicated in color. Thin solid lines, mapped faults; dashed lines, inferred faults (Fig. 1). (b) Map of relocated sequence (star, mainshock; circle, aftershock) with tomoDD method. Locations of two depth cross sections AA′ and BB′ are also shown.

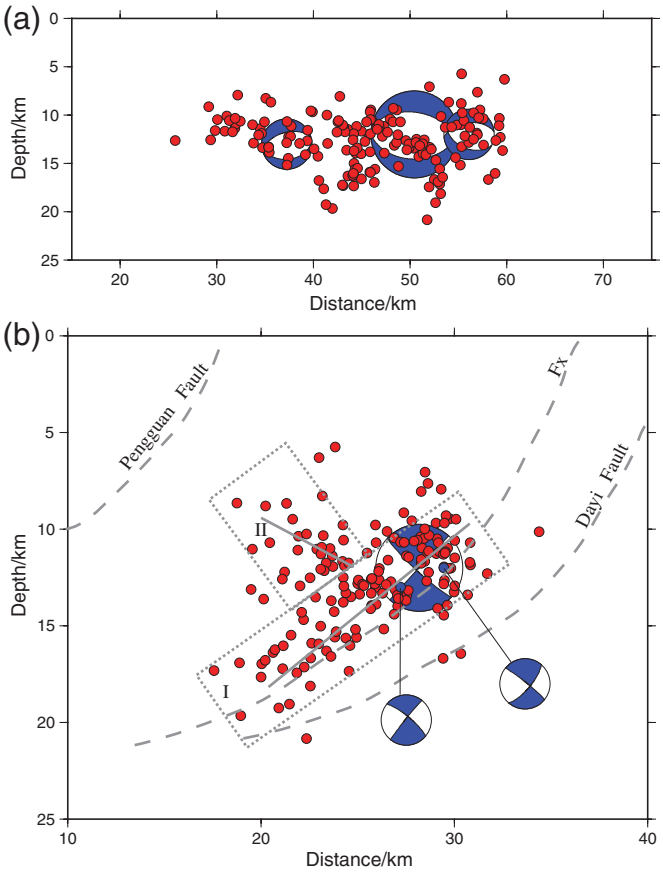

▲ **Figure 5.** Depth cross sections along (a) AA′ and (b) BB′ (see Fig. 4b). Fault-plane solutions of the mainshock and two **M**5+ aftershocks are also projected on the cross sections. Note their depths are from waveform inversions (Table 1). Dashed lines, inferred faults; dotted line boxes, two aftershock zones.

Institute of Geophysics, China Earthquake Administration and Incorporated Research Institutions for Seismology Data Management Center (IRIS DMC). Catalog and phase data were from the China Earthquake Network Center. We thank Z. L. Wu for his great suggestions and G. X. Yi for help in making figures. We also thank three anonymous reviewers for detailed and constructive comments. This research was supported by National Natural Science Foundation of China (41204045, 41274069), National Technology Support Project (2012BAK19B01), and National Key Basic Research Program of China (2013CB733203).

REFERENCES

Chang, C. H., Y. M. Wu, T. C. Shin, and C. Y. Wang (2000). Relocation of the 1999 Chi-Chi earthquake in Taiwan, *Terr. Atmos. Ocean. Sci.* **11,** no. 3, 581–590.

Chen, W. W., S. D. Ni, Z. J. Wang, X. F. Zeng, and S. J. Wei (2012). Joint inversion with both local and teleseismic waveforms for source parameters of the 2010 Kaohsiung earthquake, *Chin. J. Geophys.* **55,** no. 7, 2319–2328 (in Chinese with English abstract).

Densmore, A. L., M. A. Ellis, Y. Li, R. Zhou, G. S. Hancock, and N. Richardson (2007). Active tectonics of the Beichuan and Pengguan faults at the eastern margin of the Tibetan Plateau, *Tectonics* **26,** 1–17.

Densmore, A. L., Y. Li, M. A. Ellis, and R. Zhou (2005). Active tectonics and erosional unloading at the eastern margin of the Tibetan Plateau, *J. Mt. Sci.* **2,** no. 2, 146–154.

Hardebeck, J. L., J. Boatwright, D. Dreger, R. Goel, V. Graizer, K. Hudnut, C. Ji, L. Jones, J. Langbein, J. Lin, E. Roeloffs, R. Simpson, K. Stark, R. Stein, and J. C. Tinsley (2004). Preliminary report of the 22 December 2003, *M* 6.5 San Simeon, California earthquake, *Seismol. Res. Lett.* **75,** no. 2, 155–172.

Hauksson, E., and P. Shearer (2005). Southern California hypocenter relocation with waveform cross-correlation, part 1: Results using the double-difference method, *Bull. Seismol. Soc. Am.* **95,** no. 3, 896–903.

Hauksson, E., L. M. Jones, and K. Hutton (1995). The 1994 Northridge earthquake sequence in California: Seismological and tectonic aspects, *J. Geophys. Res.* **100,** no. B7, 12,335–12,355.

Huang, Y., J. P. Wu, T. Z. Zhang, and D. N. Zhang (2008). Relocation of the *M* 8.0 Wenchuan earthquake and its aftershock sequence, *Sci. China Earth Sci.* **51,** no. 12, 1703–1711.

Jin, W. Z., L. J. Tang, K. M. Yang, G. M. Wan, and Z. Z. Lü (2010). Segmentation of the Longmen Mountains thrust belt, Western Sichuan foreland basin, SW China, *Tectonophysics* **485,** 107–121.

Klein, F. W. (2002). User's guide to Hypoinverse-2000, a FORTRAN program to solve for earthquake locations and magnitudes, *U.S. Geol. Surv. Open-File Rept. 02-171*, 1–123.

Li, Z. W., S. D. Ni, T. Y. Hao, Y. Xu, and S. Roecker (2012). Uppermost mantle structure of the eastern margin of the Tibetan plateau from interstation *Pn* traveltime difference tomography, *Earth Planet. Sci. Lett.* **335,** 195–205.

Liu, J., G. X. Yi, Z. W. Zhang, Z. J. Guan, X. Ruan, F. Long, and F. Du (2013). Introduction to the Lushan, Sichuan *M* 7.0 earthquake on 20 April 2013, *Chin. J. Geophys.* **56,** 1404–1407 (in Chinese with English abstract).

Luo, Y., S. D. Ni, X. F. Zeng, J. Xie, Y. Chen, and F. Long (2011). The *M* 5.0 Suining–Tongnan (China) earthquake of 31 January 2010: A destructive earthquake occurring in sedimentary cover, *Chin. Sci. Bull.* **56,** 521–525.

Parsons, T., C. Ji, and E. Kirby (2008). Stress changes from the 2008 Wenchuan earthquake and increased hazard in the Sichuan basin, *Nature* **454,** 509–510.

Sibson, R. H., and G. Xie (1998). Dip range for intracontinental reverse fault ruptures: Truth not stranger than friction? *Bull. Seismol. Soc. Am.* **88,** 1014–1022.

Somerville, P., K. Irikura, R. Graves, S. Sawada, D. Wald, N. Abrahamson, Y. Iwasaki, T. Kagawa, N. Smith, and A. Kowada (1999). Characterizing crustal earthquake slip models for the prediction of strong ground motion, *Seismol. Res. Lett.* **70,** no. 1, 59–80.

Waldhauser, F., and W. L. Ellsworth (2000). A double-difference earthquake location algorithm: Method and application to the Northern Hayward fault, California, *Bull. Seismol. Soc. Am.* **90,** 1353–1368.

Wang, C. Y., W. B. Han, J. P. Wu, H. Lou, and W. W. Chan (2007). Crustal structure beneath the eastern margin of the Tibetan Plateau and its tectonic implications, *J. Geophys. Res.* **112,** B07307, doi: 10.1029/2005JB003873.

Wang, W. M., J. L. Hao, and Z. X. Yao (2013). Preliminary result for rupture process of Apr. 20, 2013, Lushan earthquake, Sichuan, *Chin. J. Geophys.* **56,** no. 4, 1412–1417 (in Chinese with English abstract).

Xie, J., S. D. Ni, and X. F. Zeng (2012). 1D shear wave velocity structure of the shallow upper crust in central Sichuan Basin, *Earthq. Res. Sichuan* **143,** no. 2, 20–24 (in Chinese with English abstract).

Xu, Z. Q., S. C. Ji, H. B. Li, L. W. Hou, X. F. Fu, and Z. H. Cai (2008). Uplift of the Longmenshan range and the Wenchuan earthquake, *Episodes* **31,** 291–301.

Yang, X. P., P. Jiang, F. M. Song, X. H. Liang, X. C. Chen, and Z. W. Deng (1999). The evidence of the South Longmenshan fault zones cutting late Quaternary stratum, *Seismol. Geol.* **21,** 341–345 (in Chinese with English abstract).

Zeng, X. F., Y. Luo, L. B. Han, and Y. L. Shi (2013). The Lushan M_S 7.0 earthquake on 20 April, 2013: A high-angle thrust event, *Chin. J. Geophys.* **56,** no. 4, 1418–1424 (in Chinese with English abstract).

Zhang, Y. Q., and H. L. Li (2010). Late quaternary active faulting along the SW segment of the Longmenshan fault system, *J. Quaternary Sci.* **30,** no. 4, 699–710 (in Chinese with English abstract).

Zhang, H. J., S. Roecker, C. H. Thurber, and W. J. Wang (2012). Seismic imaging of microblocks and weak zones in the crust beneath the southeastern margin of the Tibetan Plateau, in *Earth Sciences*, I. A. Dar (Editor), InTech Publishing, Shanghai, China, 159–202, ISBN: 978-953-307-861-8.

Zhang, P. Z., X. Z. Wen, X. W. Xu, W. J. Gan, M. Wang, Z. K. Shen, Q. L. Wang, Y. Huang, Y. Zheng, X. J. Li, Z. Q. Zhang, S. L. Ma, Y. K. Ran, Q. Y. Liu, Z. F. Ding, and J. P. Wu (2009). Tectonic model of the great Wenchuan earthquake of May 12, 2008, Sichuan, China, *Chin. Sci. Bull.* **54,** no. 7, 944–953 (in Chinese).

Zhao, L. S., and D. V. Helmberger (1994). Source estimation from broadband regional seismograms, *Bull. Seismol. Soc. Am.* **84,** no. 1, 91–104.

Zheng, Y., H. S. Ma, J. Lü, S. Ni, Y. C. Li, and S. J. Wei (2009). Source mechanism of strong aftershocks ($M_S \geq 5.6$) of the 2008/05/12 Wenchuan earthquake and the implication for seismotectonics, *Sci. China Earth Sci.* **52,** no. 6, 739–753.

Zheng, X. F., Z. X. Yao, J. H. Liang, and J. Zheng (2010). The role played and opportunities provided by IGP DMC of China National Seismic Network in Wenchuan earthquake disaster relief and researches, *Bull. Seismol. Soc. Am.* **100,** no. 5B, 2866–2872.

Zhou, Y. S., and C. R. He (2009). The rheological structures of crust and mechanics of high-angle reverse fault slip for Wenchuan M_S 8.0 earthquake, *Chin. J. Geophys.* **52,** no. 2, 474–484 (in Chinese with English abstract).

Zhu, L., and D. V. Helmberger (1996). Advancement in source estimation techniques using broadband regional seismograms, *Bull. Seismol. Soc. Am.* **86,** no. 5, 1634–1641.

Zhu, L., and L. A. Rivera (2002). A note on dynamic and static displacements from a point source in multilayered media, *Geophys. J. Int.* **148,** 619–627.

Libo Han
Changsheng Jiang
Institute of Geophysics
China Earthquake Administration
Beijing 100081, China
chinakkmm@gmail.com

Xiangfang Zeng
CAS Key Laboratory of Computational Geodynamics
University of Chinese Academy of Sciences
Beijing 100049, China

Sidao Ni
State Key Laboratory of Geodesy and Earth's Dynamics
Institute of Geodesy and Geophysics
Chinese Academy of Sciences
Wuhan 430077, China

Haijiang Zhang
School of Earth and Space Sciences
University of Sciences and Technology of China
Hefei 230026, China

Feng Long
Earthquake Administration of Sichuan Province
Chengdu 610041, China